AN ABSTRACT OF THE THESIS OF

Ali Alabdulali for the degree of Master of Science in Mechanical Engineering presented on August 31, 2023.

Title: LPBF and Post Processing of H13 Tool Steel.

Abstract approved:

_____

Somayeh Pasebani

Laser powder bed fusion (LPBF) is an innovative method where metal powder is fused together to generate complex geometries. LPBF is used as a technology to reduce material waste, and extensive labor that are often linked to conventional subtractive manufacturing. H13 tool steel is one of the widely used materials in several industries and has, therefore, gained interest in the additive manufacturing field due to its excellent mechanical properties. To produce H13 parts with optimal mechanical properties, printing parameters are optimized and a high relative density of 98% is obtained. Laser power of 203W, scanning speed of 700 mm/s, hatch spacing of 40μm and layer thickness of 25 μm are used to obtain the optimal results. Hot isostatic pressing is applied to cure the microcracks and has shown a 0.5% increase in the relative density, while it showed a significant decrease in other samples due to the excessive residual heat. Optical and scanning electron microscopy are used to observe the recrystallization of grains and grain growth resulted by tempering and rapid cooling. Tempering temperatures of 650˚C resulted in a greater reduction of microhardness than 550 ˚C. While high hot isostatic pressing temperature (1163 ˚C) shows a worsening effect on the microstructures.

LPBF and Post Processing of H13 Tool Steel

by
Ali Alabdulali

A THESIS

submitted to

Oregon State University

in partial fulfillment of
the requirements for the
degree of

Master of Science

Presented August 31, 2023.
Commencement June 2024

Master of Science thesis of Ali Alabdulali presented on August 31, 2023

APPROVED:

Major Professor, representing Mechanical Engineering

Head of the School of Mechanical, Industrial, and Manufacturing Engineering

Dean of the Graduate School

I understand that my thesis will become part of the permanent collection of Oregon State University libraries. My signature below authorizes release of my thesis to any reader upon request.

Ali Alabdulali, Author

ACKNOWLEDGEMENTS

I, the author, express sincere appreciation for the encouragement, patience and support I received from my advisor, Dr. Pasebani. Without your help, this would not have been possible.

I am thankful to my colleagues Kuba (Jakub) Preis, Stephanie Lawson, Seong Yang, and Nahal Ghanadi for their support during my two-year journey at Oregon State University.

I would like to thank Dr. Milad Ghayoor for training on lab equipment that was of tremendous help to complete this thesis.

I am thankful for my committee members Dr. Megumi Kawasaki, Dr. Donghua Xu, Dr. Hisham Jashami who took their valuable time to evaluate my defense.

I would also like to thank the School of MIME for their GTA appointment. Especially, Dr. Oman whom I worked with for the entire duration of my 2-year program. I learned valuable lessons from Dr. Oman's expertise, and for that I am thankful.

Thank you to the Oregon Manufacturing and Innovation Center (OMIC) for funding my project.

Finally, I am beyond thankful to my family's unconditional love and support. My wife's support was a major factor in the progress I've made. My mother's long phone calls kept me motivated, despite the long distance and long years that I have

not seen her. Without my family's support, this would have been more difficult. Thank you.

TABLE OF CONTENTS

LIST OF FIGURES

Figure Page

LIST OF FIGURES(Continued)

Page

LIST OF TABLES

Chapter 1. Introduction

1.1 Background

Metals and alloys have been used to fabricate parts throughout history. The origin of alloys, the combination of two or more metal elements, is traced back to the Iron Age. The Iron Age took place in the Caucasus region in 2000 BCE, roughly 4,022 years ago [1]. Alloys can be altered by combining specific elements that exhibit certain behaviors to achieve desired alloy properties. For example, tungsten has the highest melting temperature and by combining it with other elements, an alloy with hot temperature application can be fabricated [2]. Thus, understanding the alloy composition is crucial for achieving optimal results for a specific application.

In the industrial field, extrusion molds and dies undergo severe amounts of thermal fatigue, wear, and erosion. These effects lead to a shorter lifetime of the parts, and as a result a negative impact on production cycles. A suggested mitigation measure is to use an alloy with excellent thermal resistance, toughness, and strength. One of the best candidates for this application is H13 tool steel [3]. To achieve the desired qualities, H13 tool steel is used for its chemical composition that consists of carbon(C), silicon (Si), vanadium(V), chromium (Cr), molybdenum (Mo), manganese (Mn), and iron (Fe).

The addition of elements is known as microalloying, where it has been discovered that the presence of Cr and V in H13 reduces corrosion rates [4]. In the case of V addition, it was found that the microhardness is highly affected by the weight percentage of V. H13 alloys with low V weight percentage showed higher microhardness values than those with high V weight percent [5]. Hence, the weight percentage of elements in an alloy is another critical factor in achieving desired mechanical properties.

Conventional manufacturing (CM) practices, such as machining, injection molding and die-casting have been used throughout time in different industries. CM practices are best when it comes to high volume, simple-geometry production in terms of cost

effectiveness and time. However, a more innovative manufacturing practice is needed to meet the high complexity of geometrical requirements as well as the varying alloy compositions. Additive Manufacturing (AM) was first developed in the 1960s and has made tremendous growth in the manufacturing field. One advantages and advancement of AM over CM is the design-freedom and wide selection of metal powder used to manufacture alloys [6].

CM is a process in which material is subtracted from an existing part to produce a specific geometry. Conversely, AM is a process where material is added in a layer-by-layer fashion to reach a pre-designed geometry using a computer aided design (CAD) [7]. One of the many different technologies of AM is known as Selective Laser Melting (SLM), also referred to as Laser Powder Bed Fusion (LPBF). In LPBF, a laser is used to melt powder to a specified shape in a sequential manner until the part is completely manufactured [7].

Within LPBF, different parameters play a major role in the quality and geometrical integrity of any manufactured part. These parameters are of high interest because they directly affect the quality of the parts produced via LPBF. Parameters such as laser power, scanning speed, layer thickness (LT), and hatch spacing (HT) highly affect the porosity, density hardness, and other mechanical properties of a part [8].

Since AM is a relatively new technology, some additional work is often required to enhance the properties of a manufactured part [6]. A crucial step in achieving a high-quality manufactured part is known as post processing. Post processing may include some of the following methods, rolling operations, water quenching, tempering, and hot isostatic pressing (HIP). The goal of post processing is to improve the mechanical properties and the subsurface properties [9-10]. Current research in the field is investigating different manufacturing parameters, as well as post processing techniques to achieve optimal results using H13 powder via LPBF [11].

The focus of this thesis will be on process parameter optimization for H13 tool steel powder via laser powder bed fusion technology. A total of 27 different printing parameter combinations/sets are explored in the search to find the optimal mechanical properties/outcomes associated with each set. Hot isostatic pressing followed by heat

treatment (HT), including rapid cooling and tempering, are also evaluated to examine the microstructural changes.

1.2 Objectives and Motivations

With varying parameter sets and post processing techniques, the objective of this thesis is to explore new parameters and post processes on H13 tool steel using LPBF. The novelty of this thesis is in new chosen parameters and the post processing techniques apply on additively manufactured H13 tool steel using LPBF.

The following chapter focuses on the results associated with 27 different parameter sets followed by hot isostatic pressing, rapid cooling and tempering of H13 cubic samples.

One of the advantages of AM is the ability to manufacture complex geometries with minimal supervision in a singular print, as opposed to manufacturing separate parts that would need to be assembled as seen in CM [6]. To fully benefit from the advantages of AM, researchers aim to draw connections between printing parameters and resulting mechanical properties. Thus, the processing parameters and the effects of post processing techniques on microhardness, density and microstructures are documented.

1.3 Literature Review

Due to the nature of traditional manufacturing, often metals are heated to a liquid state then are poured into a container, a mold for instance, to produce a certain geometry. The following subsection provides an insight on how molds and dies are used and why it is important for them to possess the quality they have.

1.3.1. Die-casting in the manufacturing industry

Metal parts such as nuts, bolts, wrenches, and rods play a major role in the integration of most equipment, appliances, automobiles, and devices in our daily life [29]. Simple-geometry parts are produced in large quantities. The production of a bolt, for instance, requires a tool and a technique that would take into consideration the small details present in a bolt. Die casting is a popular technique used for the mass production of metal parts that require accuracy and repeatability [30]. The technique is cost effective, accurate, and efficient in the production of large quantities of parts having simple geometry. The following paragraph illustrates the mechanism of die-casting.

A study conducted by Lee et al. focused on the process of die-casting and is illustrated in Figure 1. [30]. The process of die-casting to produce a metal part, as highlighted by Lee et. al, is explained in the following five steps:

- Step one, molten metal is melted in a furnace until it reaches a liquid form.
- Step two, the molten metal is then poured into the gap by the plunger.
- Step three, the plunger pushes the molten metal into the die cavity until it is filled.
- Step four, the ejector die retracts while the cover dies remains stationary.
- Step five, ejector pins move to push out the finished product.

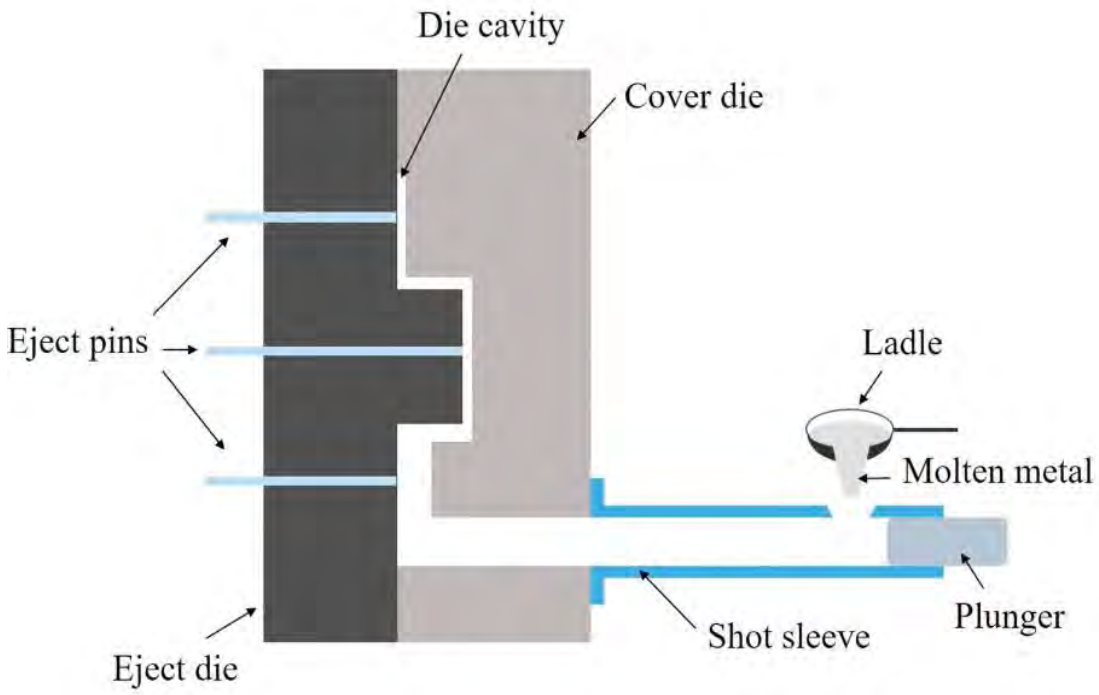

Figure 1.1: the mechanism of die-casting of molten metal [30]

As seen in Figure 1.1, the die-casting mold has specific features such as the eject pins and the die cavity. These features determine the final shape of the manufactured product. Therefore, the mold itself needs to be resistant to any damage caused by heat since the temperature of the molten metal can reach up to 700˚C [31]. Otherwise, the desired shape produced via die-casting cannot be reached due to the damage in the mold itself.

1.3.2. H13 tool steel history and importance

Molds and dies have been essential tools in many industries. They are traced back to the 1920s, when the automobile industry started to expand. The quality of dies and molds in the automobile industry are crucial in ensuring the high quality of manufactured car parts. It is estimated that several thousands of molds and dies are necessary to produce a single automobile [12]. Several industries rely heavily on molds and dies, as they are essential in forming glass, rubber metals and plastics.

Due to their heavy usage, the quality of dies and molds are crucial for the success of part production. A study done by Coldwell et. al, looked at the rapid machining of AISI H13.Iit was concluded that H13 is one of the most used alloys in the production of molds and dies [13]. Prior to AM, subtractive methods were used to create molds and dies. Some examples of subtractive manufacturing and their techniques will be discussed in the following subsection.

1.3.3 H13 in conventional manufacturing

Prior to AM, subtractive methods were used to create mold and die. Drilling, sawing, cutting, tapping, and forging are some examples of subtractive manufacturing.

In one case study by Coldwell, Helen, et al., the drilling and cutting of H13 components was carried out using different drilling/cutting parameters. The goal of the study was to highlight causes of part failure. The study concluded that when standard drill bits were used, higher rates of failure occurred. Chipping of drilling/cutting tools was a common failure due to the high hardness nature of H13. The use of AlTiN coated carbide tools along with soluble oil cutting fluid was a necessary measure in reducing failure rates when drilling/cutting H13 components [13].

Another case study by Harihaaran et. al focused on the manufacturing of H13 materials using a method known as computer numerical control (CNC), in which a drill moves automatically in the XYZ direction. The directions are generated by a G-code and allow for less human-machine interaction [14]. H13 die steel using CNC machining was examined [14]. The study showed CNC machining is another common method of working with H13. The use of carbide coated drills is essential in preventing drills from premature fractures or chipping. Otherwise, fractures of cutting tools were common when standard uncoated drill bits were used.

Hybridization or the use of combining different manufacturing techniques is another common practice when dealing with tool steel [15]. The purpose of combining different manufacturing methods is seen effective in the production of parts of high complex geometries, but hybridization was found to be labor, energy, and equipment intensive [16].

A more recent method used to manufacture materials of high hardness such as tool steel is known as electrical discharge machining (EDM). In EDM, a series of sparks between a metal wire and the workpiece is generated. A current passes through the wire, which leads to an electric spark in the wire. With the addition of dialectic fluid, the current in the wires cuts the material in the workpiece without making direct contact. The reason EDM is widely used is because it is highly effective in cutting material with a high hardness [17]. Even though EDM is an effective method in cutting tool steel, it is time intensive and is an ineffective technique against non-conductive materials. Another disadvantage of EDM is related to the current (amperage) used to cause the electric discharge. In a literature review, Guu et. al found that the pulse current used to cut materials in EDM can lead to two possible failures. When pulse current was set too high, melting of materials was found. Too low of a pulse current led to void and keyholes in the manufactured parts on the edges [17].

Subtractive or conventional manufacturing methods of H13 have limitations due to the mechanical properties of the alloy. Examples of the challenges are the need for coolants and carbide coated tools to prevent chipping during manufacturing, intensive labor and energy requirements, and slow cutting rates as seen in EDM. Other challenges and advances in the additive manufacturing industry will be discussed in the following subsection.

1.3.4 additive manufacturing – various techniques

The ISO/ASTM 52900 standard [18] categorizes additive manufacturing into seven main categories [19]: binder jetting, sheet lamination, direct energy deposition (DED), material extrusion, material jetting, vat polymerization, and laser powder bed fusion (LPBF). Perez et al. [19] highlight several advantages and disadvantages associated with AM technologies. The advantage of AM are as follows:

- Fully automated process.
- Complex geometries achieved without extra costs in production.
- Inner features, lattices, and cooling channels.
- Complete manufacturing in a single print.

Conversely, Perez et al, state that the current performance of AM is not comparable to the performance of conventional manufacturing. For instance, one defect found in additively manufactured parts is poor surface finish. The parameters that affect surface finish are layer thickness, part orientation, and deposition of material [20]. However, with parameter optimization, AM technologies can achieve promising results. The following subsection defines the DED process and discusses the defects and challenges associated with direct energy deposition (DED) method using tool steel powder.

1.3.5 additive manufacturing – DED

In 1986, Carl Deakard and Joseph Beaman patented a process known as selective laser sintering (SLS). Based on that process, direct energy deposition was later invented [21, 22]. The process of DED, as stated by the ASTM 52900 standard [18], can be summarized as: the melting and fusion of material via focused thermal energy, such as laser, through a nozzle and onto a substrate as shown in Figure 1.2 below.

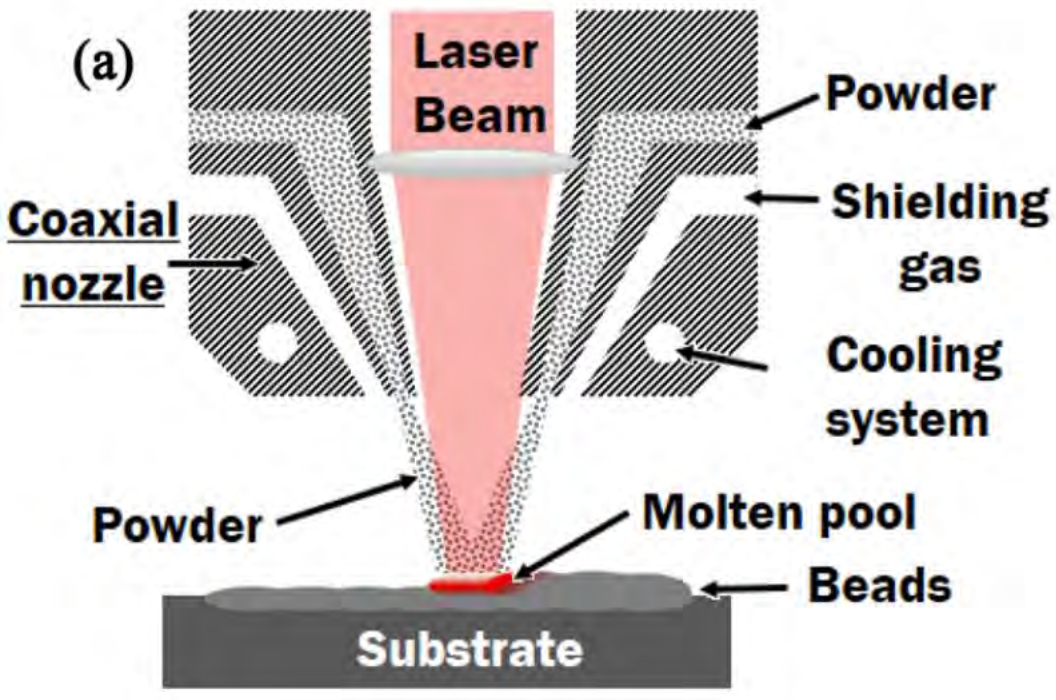

Figure 1.2: illustration of DED [21]

The main purpose of DED is to fabricate metallic parts in a layer-by-layer manner with a near-net shape [21]. However, recently the DED process has expanded to other applications such as damage repair, porous coating, and thermal management [23-25]. In other words, DED can be used to repair and remanufacture existing parts as opposed to full-scale manufacturing from the ground up.

In DED, several parameters were found to have an influence on the quality of the manufactured part. The main parameters are powder feed rate, and the laser spanning speed [26]. Craig et. al, conducted an experiment on DED using H13 tool steel powder with the goal of process optimization. In their literature, they concluded that a slow scanning speed (400- 500 mm/min) resulted in overbuilding of material, and in porosities as shown in Figure1.3.

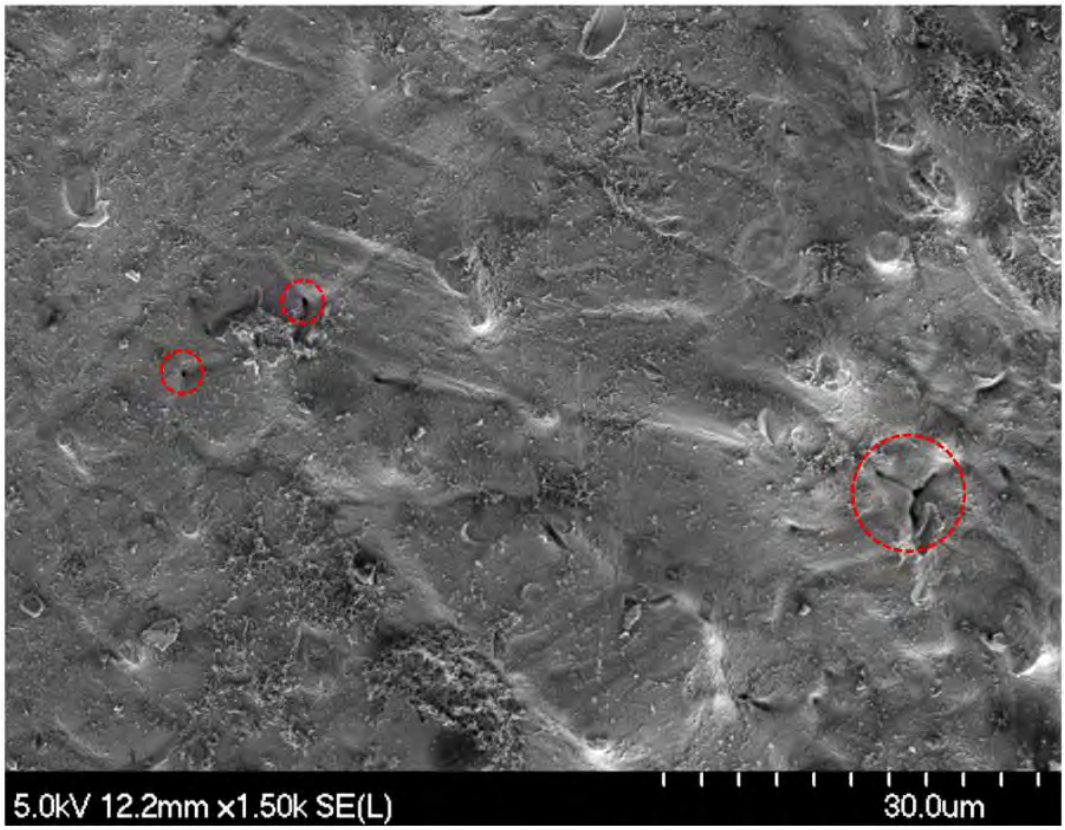

Figure 1.3: porosity in printed H13 sample fabricated using DED shown in red circles [26].

Other researchers found other challenges in the DED process. Dass et. al, summarized a list of defects associated with the DED process. Unwanted phase transformation, pore content, grain growth, and residual stresses are all current challenges the AM industry faces [27]. These defects were resulted by rapid cooling rates, extreme heating, and rapid solidification of particles during the DED process [21]. The following subsection discusses another method in the AM industry, LPBF, as well as a project. This project was led and funded by the Oregon Manufacturing and Innovation Center (OMIC). The completion of this thesis was also funded by OMIC.

1.3.6 Tool steel- LBPF Boring Bar

LPBF is a process where powder is moved from a powder reservoir into a build plate. The powder in the build plate is placed under a Lense of which a laser beam targets the powder in the build plate. The laser beam melts and fuses the powder to generate the desired shape [27]. The parameters that affect the LPBF process are: scanning speed, laser power, hatch spacing and layer thickness.

Professors and students from Oregon State University collaborated with OMIC on an innovative project. The project's objective was to use AM to fabricate a boring bar with internal dampers. The internal dampers had small details that would not be easily manufactured through any conventional method, making AM a more suitable option. Figure 1.4 below shows a sketch of the damper section of the boring bar. An open cross-section was made to reveal the inner dampers.

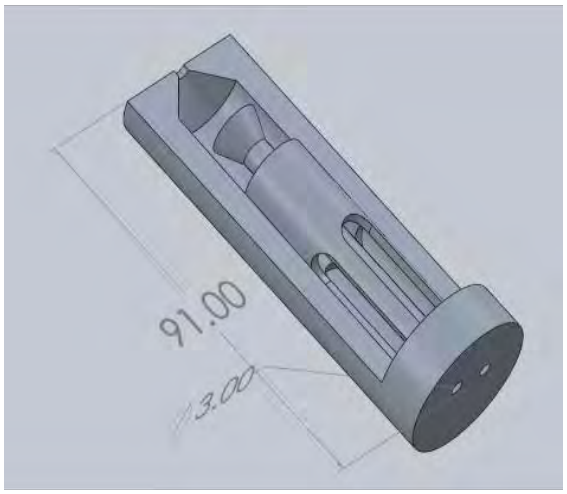

Figure 1.4: Cross-section boring bar showing the inner dampers.

304L stainless steel powder was used to produce the boring bar. The parameters for 304L were optimized by Ghayoor et. al [28]. The optimized parameters for 304L steel via LPBF are scanning speed of 300 mm/s, laser power of 145W, hatch spacing of 50 μm, and layer thickness of 30 μm. Ghayoor et. al, conducted their experiment using a solid cylindrical part, and found that the optimized parameters resulted in a relative density of >99%.

The optimized parameters were used to produce the boring bar. Different printing orientations were also tested. Results are discussed in the next paragraph, and the different orientations are shown in figure 1.5 below.

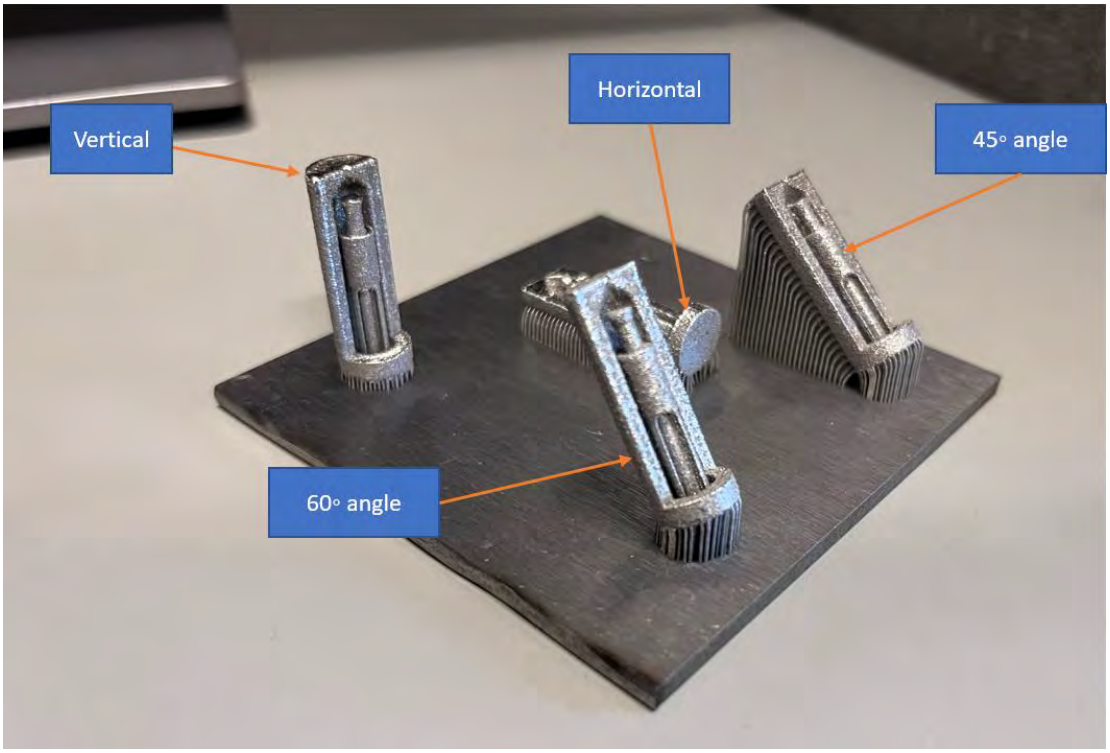

Figure 1.5: printed boring bars at 4 different orientations.

During the printing processing, it was observed that the horizontal printing reduced the print time and powder consumption by roughly 50% in comparison to the vertical orientation. However, the accumulated heat in the horizontal orientation caused visible distortion and wrappage as shown in figure 1.6 below. Also, the internal features were not successfully obtained as the internal dampers melted due to excessive heat.

Figure 1.5: horizontal printing showing material distortion.

On the contrary, angled and vertical orientation had less distortion and the internal dampers were printed successfully as shown below in figure 1.6.

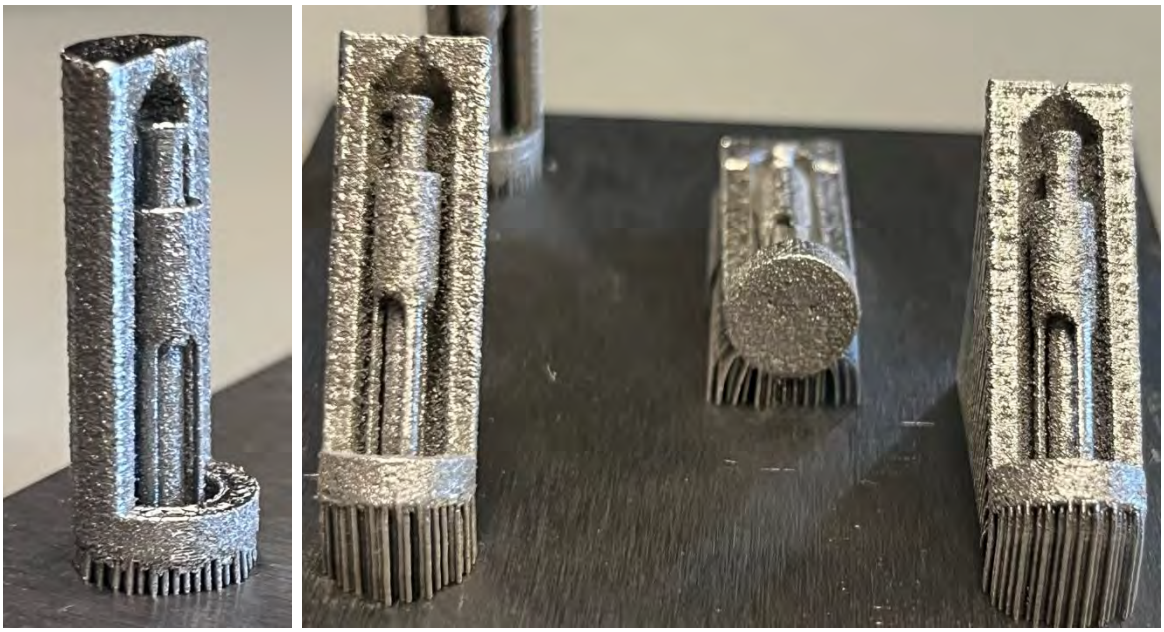

Figure 1.6: vertical and angled orientations of boring bars

Although the internal dampers were successfully printed, the surface roughness was high. The highest obtained relative density was 96.7%, which did not match the relative density obtained from the literature [28].

The discrepancies in results can be attributed to the difference in geometry. In experiment of Ghayoor et.al, a solid cylindrica shape was used to obtain the >99% relative density. Nonetheless, the boring bar's geometry was more complex and had internal features. Further investigation is needed to better understand the discrepancies.

References

[1] Spoerl, Joseph S. "A brief history of iron and steel production." (2004).

[2] Wang, Yanlin, Longchao Zhuo, and Enhuai Yin. "Progress, challenges and potentials/trends of tungsten-copper (WCu) composites/pseudo-alloys: Fabrication, regulation and application." *International Journal of Refractory Metals and Hard Materials* 100 (2021): 105648.

[3] Yang, Xin, et al. "Microstructure evolution and mechanical properties of H13 steel produced by Selective Electron Beam Melting." *Materials Characterization* (2023): 113053.

[4] Edmonds, David V., and Robert C. Cochrane. "The effect of alloying on the resistance of carbon steel for oilfield applications to CO2 corrosion." *Materials Research* 8 (2005): 377-385.

[5] Chen, Xuebin, et al. "Effect on Microstructure and Mechanical Properties of Microwave-Assisted Sintered H13 Steel Powder with Different Vanadium Contents." *Materials* 15.4 (2022): 1273.

[6] Pereira, Tanisha, John V. Kennedy, and Johan Potgieter. "A comparison of traditional manufacturing vs additive manufacturing, the best method for the job." *Procedia Manufacturing* 30 (2019): 11-18.

[7] Liu, Guo, et al. "Additive manufacturing of structural materials." *Materials Science and Engineering: R: Reports* 145 (2021): 100596.

[8] Yadroitsev, Igor, Ph Bertrand, and I. Smurov. "Parametric analysis of the selective laser melting process." *Applied surface science* 253.19 (2007): 8064-8069.

[9] Breidenstein, Bernd, et al. "Effect of post-process machining on surface properties of additively manufactured H13 tool steel." *HTM Journal of Heat Treatment and Materials* 73.4 (2018): 173-186.

[10] AlMangour, Bandar, Dariusz Grzesiak, and Jenn-Ming Yang. "Selective laser melting of TiB2/H13 steel nanocomposites: Influence of hot isostatic pressing post-treatment." *Journal of Materials Processing Technology* 244 (2017): 344-353.

[11] Yuan, Miwen, et al. "Characteristics of a modified H13 hot-work tool steel fabricated by means of laser beam powder bed fusion." *Materials Science and Engineering: A* 831 (2022): 142322.

[12] Baba, Toshiyuki. "Progress of the dies and molds industry and the role of the German immigration network in Brazil: Case studies in ABC districts in Sao Paulo, Resende, and Joinville." (2018).

[13] Coldwell, Helen, et al. "Rapid machining of hardened AISI H13 and D2 moulds, dies and press tools." *Journal of Materials Processing Technology* 135.2-3 (2003): 301-311.

[14] KB, Hariharan, et al. "Effects of machining parameters on H13 die steel using CNC drilling machine." *Composites and Advanced Materials* 32 (2023): 26349833231189296.

[15] Grzesik, Wit. "Hybrid additive and subtractive manufacturing processes and systems: a review." *Journal of Machine Engineering* 18.4 (2018): 5-24.

[16] McHugh, K. M., et al. "Influence of cooling rate on phase formation in spray-formed H13 tool steel." *Materials Science and Engineering: A* 477.1-2 (2008): 50-57.

[17] Guu, Y. H., et al. "Effect of electrical discharge machining on surface characteristics and machining damage of AISI D2 tool steel." *Materials Science and Engineering: A* 358.1-2 (2003): 37-43.

[18] ISO/ASTM 52900: Additive manufacturing. General principles. Terminology. ISO/ASTM 2015.

[19] Pérez, Mercedes, et al. "Current advances in additive manufacturing." *Procedia Cirp* 88 (2020): 439-444.

[20] Boschetto, Alberto, and Luana Bottini. "Roughness prediction in coupled operations of fused deposition modeling and barrel finishing." *Journal of Materials Processing Technology* 219 (2015): 181-192.

[21] Ahn, Dong-Gyu. "Directed energy deposition (DED) process: State of the art." *International Journal of Precision Engineering and Manufacturing-Green Technology* 8 (2021): 703-742.

[22] Frazier, William E. "Metal additive manufacturing: a review." *Journal of Materials Engineering and performance* 23 (2014): 1917-1928.

[23] Ahn, D. G. (2016). Direct metal additive manufacturing processes and their sustainable applications for green technology: A review. International Journal of Precision Engineering and Manufacturing-Green Technology, 3(4), 381–395.

[24] Yang, Dong-Yol, et al. "Flexibility in metal forming." *Cirp Annals* 67.2 (2018): 743-765.

[25] Oh, W. J., et al. "Effect of groove shapes on mechanical properties of STS316L repaired by direct energy deposition." *Transactions of Materials Processing* 29.2 (2020): 103-112.

[26] Craig, Owen, Alexandre Bois-Brochu, and Kevin Plucknett. "Geometry and surface characteristics of H13 hot-work tool steel manufactured using laser-directed energy deposition." *The International Journal of Advanced Manufacturing Technology* 116.1-2 (2021): 699-718.

[27] Katancik, Michael, et al. "Selective laser melting and tempering of H13 tool steel for rapid tooling applications." *Journal of Alloys and Compounds* 849 (2020): 156319.

[28] Ghayoor, Milad, et al. "Thermal stability of additively manufactured austenitic 304L ODS alloy." *Journal of Materials Science & Technology* 83 (2021): 208-218.

[29] Fontana, Flavia, et al. "Nuts and bolts: microfluidics for the production of biomaterials." *Advanced Materials Technologies* 4.6 (2019): 1800611.

[30] Lee, Jeongsu, Young Chul Lee, and Jeong Tae Kim. "Migration from the traditional to the smart factory in the die-casting industry: Novel process data acquisition and fault detection based on artificial neural network." *Journal of materials processing technology* 290 (2021): 116972.

[31] Niu, Zhichao, et al. "Effect of high pressure die casting on the castability, defects and mechanical properties of aluminium alloys in extra-large thin-wall castings." *Journal of Materials Processing Technology* 303 (2022): 117525.

Chapter 2. LPBF and Post Processing of H13 Tool Steel

Abstract

Laser powder bed fusion (LPBF) is an innovative method in which metal powder is fused together to generate complex geometries. LPBF is a technology used to reduce material waste, and extensive labor that are often linked to conventional subtractive manufacturing. H13 tool steel is one of the widely used materials in several industries and has, therefore, gained interest in the additive manufacturing field due to its excellent mechanical properties. To produce H13 parts with optimal mechanical properties, printing parameters are optimized and a high relative density of 98% is obtained. In this experiment, a laser power of 203W, scanning speed of 700 mm/s, hatch spacing of 40μm and layer thickness of 25 μm were used to obtain the optimal results. Hot isostatic pressing was later applied to cure the microcracks. This method showed a 0.5% increase in the relative density, while it showed a significant decrease in other samples' relative densities due to the excessive residual heat. Optical and scanning electron microscopy were used to observe the recrystallization of grains and grain growth resulted by tempering and rapid cooling. Tempering temperature of 650˚C resulted in a greater reduction of microhardness than 550 ˚C. While the hot isostatic pressing temperature (1163 ˚C) showed a worsening effect on the microstructures.

2.1 Introduction

Metals and alloys are essential components in our daily life. They are widely used in the field of automotive, aerospace, medical, construction, and tooling. As the world's population grows, the demand for more material is growing exponentially. It is predicted that by 2050, the world's demand for material, including metals, will be roughly180 billion tons (three times the current demand for material) [1]. As the demand for materials grows, waste rates are growing even higher. It is estimated that the world's current solid waste is about 2 billion tons, and it is estimated to reach 3.4 billion tons by 2050 [2].

Manufacturing of parts is essential, and material waste is an inevitable byproduct. The nature of manufacturing, nonetheless, plays a significant role in the

amount of waste generated. For instance, conventional manufacturing (CM), which is of a subtractive nature, is a method where material is removed from an existing part to reach a specific geometry. CNC machining, drilling, milling, and sawing are all examples of subtractive manufacturing. In one case study, the production of a turbine with a volume of 406 cm^3 was investigated. It was concluded that 87% of its initial volume was removed [3]. When considering the energy, cooling fluids and labor going into subtractive manufacturing, it is apparent that there is a need for a more sustainable method in the manufacturing industry.

Additive Manufacturing (AM) is an innovative method that has grown substantially in the past few decades [4]. Some of the reasons AM has gained attention is because it generates less waste than CM, less human interaction is required than CM, it can generate highly complex geometries, and it has a wide range of design and material freedom [3]. Currently, AM is widely used in many different industries including, but not limited to architecture, aerospace, medical, and automotive industry [5].

Several industries require the use of molds and dies to manufacture parts using different techniques. For example, injection molding, drilling, boring, and threading are widely used to fabricate parts of simple geometry such as bolts [6]. Tool steel is a material that is often used for such purposes due to its excellent mechanical properties.

H13 tool steel is an alloy that exhibits excellent hardness, toughness, and thermal resistance [7]. Its powder form allows H13 to be utilized in some of the AM techniques. One of the AM techniques, laser powder bed fusion (LPBF), will be investigated in this study. Several factors affect the formation of microstructures in the manufactured part. The main parameters used to manipulate the part fabrication are laser power, scanning speed, layer thickness (LT), and hatch spacing (HS).

LPBF is a relatively new technique that is still in its developing stages. Parts generated using LPBF are often accompanied with several defects such as keyholes, lack of fusion, and porosity [8]. To utilize LPBF to its full potential, a solid understanding of the process parameters and defects is needed.

This paper presents a study on LPBF process parameter optimization using H13 tool steel powder. Laser power, scanning speed, LT, and HS were altered and the effects on the manufactured part were inspected. Heat treatment and hot isostatic pressing (HIP) were also applied as post-processing methods to further eliminate the defects.

2.2 Experimental Methods

2.2.1 H13 Powder Feedstock Characterization

Carpenter Technology is one of the many vendors for metal powder. ASTM H13 tool steel powder was designed by Carpenter with a range of different particle sizes. In this experiment, H13 tool steel powder with a particle size of 30 μm was selected. A chemical composition is obtained from the vendor and is shown in Table 2.1. To compare the given chemical composition from the vendor, FEI Quanta 600F electron microscopy (SEM) was used. A comparison between the chemical composition of the powder and printed part was obtain. An energy dispersed x-ray spectroscopy (EDS) was utilized to verify the chemical composition. Table 2.2 shows the chemical composition as obtained from the Quanta 600F SEM from Oregon State University.

Table 2.1
Chemical Composition of H13 powder generated by the powder vender, Carpenter [9]

Element	Fe	Si	V	Mo	Cr	C
Wt.%	Balance	0.8-1.2	0.8-1.15	1.1-1.5	4.8-5.5	0.35-0.42

Table 2.2
Chemical Composition of H13 powder generated by EDS.

Element	Fe	Si	V	Mo	Cr
Wt.%	89.32	0.82	1.57	2.21	6.08

2.2.2 Sample Preparation

A total of 27 cubical samples were prepared using fresh powder, as opposed to recycled, from Carpenter. The printing parameters were optimized using OR Laser Creator (LPBF). The parameter ranges are as follows, laser power of 130 - 225W and scanning speed of 300 – 1,000 mm/s. Layer thickness and hatch spacing were kept constant at 25 μm, and 40 μm, respectively. A summarized table of the parameters is listed below in Table 3. The samples processing parameters varied, but their geometrical dimension remained constant at 10mm x 10mm x 5mm (W*L*H). The geometry was prepared using Solidworks, a Computer Aided Design (CAD) software. Then, a G-code was necessary to input into the OR Laser Creator. To generate the G-code, ORLAS Suite was used.

Once the G-code was successfully added to the LPBF machine, a vacuum was necessary to ensure no excess oxygen was present in the chamber to avoid impurities in the fusion process. A built-in sensor indicates the oxygen level, and it is crucial to run the printing process at oxygen level of 0.01%. To avoid overheating, an inert gas must be flowing while an extraction inlet is open. Figure 2.1 shows the human machine interface (HMI) of the LPBF machine.

Table 2.3
Summary of the parameter values being optimized.

Parameters	**Numerical Values**
Power (W)	152, 160, 177,180, 190, 203, 225
Scanning Speed(mm/s)	300, 400, 500, 600, 700, 800, 900, 1000
Hatch Spacing (μm)	40
Layer Thickness (μm)	25

Figure 2.1 HMI screen of LPBF machine indicating oxygen level, temperature, inert gas, and extraction

Using proper personal protective equipment (PPE), a manual loading of powder was necessary for the completion of each print. Figure 2.2 shows the LPBF in its printing process. (A) shows the powder reservoir where H13 powder is loaded. The reservoir, (A), moves in an upward motion to allow the re-coater, (E), to move the powder to the build plate, (B). The laser beam, (D), moves at a given power/speed and the powder is melted into a predetermined shape, (C).

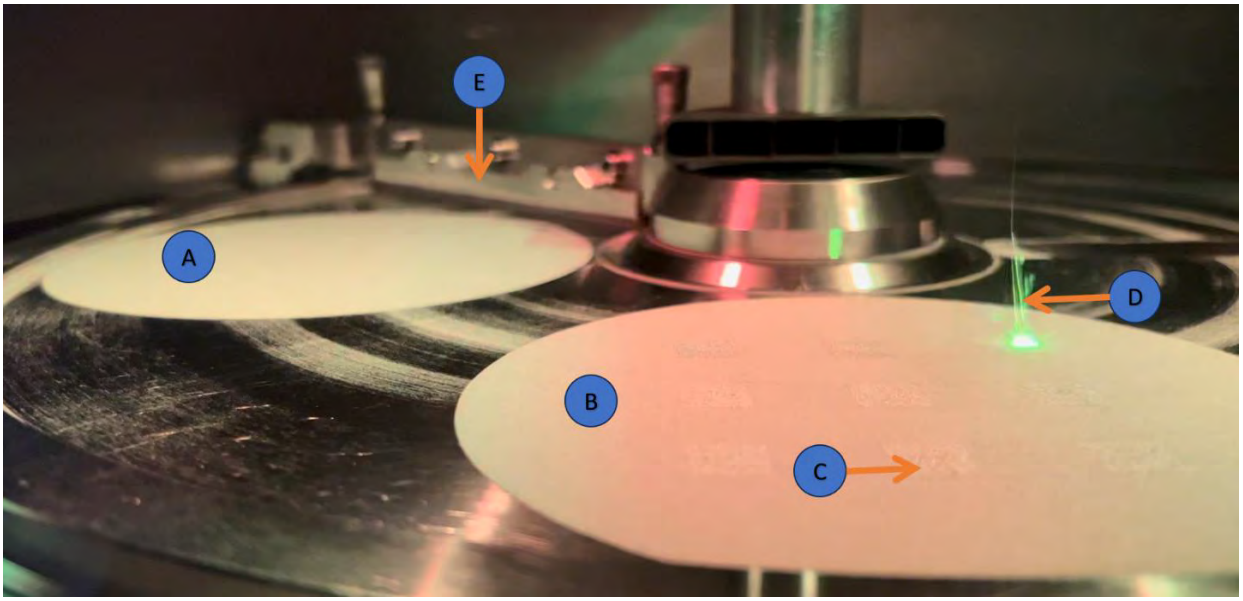

Figure 2.2: LBPF in action, where (A) indicates the powder reservoir, (B) is the build plate, (C) is the printed part, (D) is the laser beam, and (E) is the coater.

Once a printing cycle is complete, the build plate needs to be manually lifted via the HMI to expose the printed parts, followed by manual removal of parts. Figure 2.3 below shows the build plate with the printed samples after a completed printing cycle.

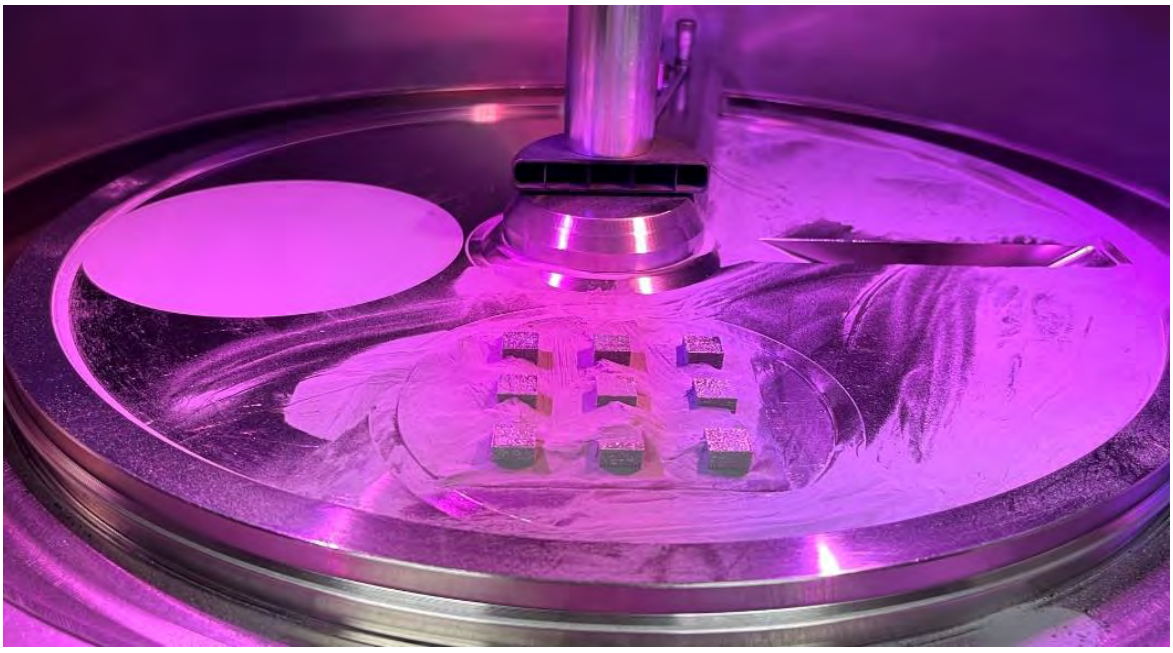

Figure 2.3: a completed print cycle before removal of the samples from the LPBF machine.

2.2.3 Post Processing and Heat Treatment

Hot isostatic pressing (HIP) was performed on the samples in a closed vessel. A temperature value of 1163℃, a pressure of 102 MPa were used for a period 3 hours to complete the HIP process. The HIP process was completed at the Oryx Advanced Materials in Malaysia, then was followed by two different heat treatments.

After HIP, the samples were heated to 1160℃ in a furnace and were kept for 2 hours followed by water quenching. Three of the five hot isostatically pressed samples were selected for additional heat tempering following the water quenching. Tempering of the samples was done at three different tempering setups: 1 hour at 550℃ followed by another hour at 650℃, 2 hours at 550℃, and 2 hours at 650℃. The ramping rate for the heating cycle was 5℃/minute, and all three samples were cooled inside the furnace and were brought back to room temperature.

2.2.4 Property Measurements

Sample density was measured by the Ohaus density scale shown in figure 2.4. The formula for density measurement was provided in the scale's manual and is as follows:

$$\rho = \frac{A}{A-B}(\rho_o - \rho_L) + \rho_L \ ,$$

In this formula, "ρ" is density, "ρ_o" is the density of water (1 g/cm^3), "ρ_L" is the density of air (0.0012 g/cm^3), "A" is the weight of sample in air, and "B" is the weight of sample in liquid. Once the density values were obtained, they were divided by the H13 numerical density value 7.73g/cm^3 which was obtained from the literature [10], to obtain the RD of each sample.

Figure 2.4: OHAUS density scale.

To measure the microhardness, the samples needed to be mounted and polished. Metallographic mounting, grinding and polishing procedures were followed to prepare the samples for microhardness measurements. The microhardness was measured using LECO LM248AT Micro-indentation Hardness Tester shown in figure 2.5. The microhardness values were recorded at 500g force and 15 second dwell time. Each sample was indented and measured 10 times, at different locations across the sample.

Figure 2.5: LECO LM248AT Micro-indentation Hardness Tester

The microstructures were exposed using an etching solution. 2 vol% nital solution was prepared by mixing 2mL of nitric acid with 98mL of ethanol according to a procedure obtained from another study [10]. Each sample was submerged in the nital solution for a period ranging from 1 to 3 minutes. The length of submerging was determined by the exposure of the microstructural details, which was examined by an optical microscope.

2.2.6 Microstructure Analysis

After sample mounting and polishing, initial images were taken using Zeiss Axitron optical microscope to ensure full exposure of grain boundaries was obtained. A scanning electron microscope (SEM) was needed to capture the microstructures. FEI Quant 600F SEM was used to analyze microstructural changes and defects. An EDS was used to analyze the chemical composition of H13 samples and the distribution of elements.

2.3 Results and Discussion

2.3.1 H13 process optimization

Heat treatment and HIP for all 27 samples was unnecessary due to the large number of samples. An elimination process of unwanted results was taken to narrow down the experiment. The relative density of as-printed samples was the first justification for choosing what sample to proceed with and apply HIP and heat treatment. Figure 2.6 below shows the power/speed values and their corresponding RDs, where the values ranged from 91% to 97%.

Only five samples with the highest RD values, as circled in red in figure 2.6, were selected to proceed in this experiment. Another factor for selecting the sample is their volumetric energy density (VED), where it has shown that the samples of high VED (above 300 J/mm^3) exhibited cracks and keyhole, while samples with low VED (below 200 J/mm^3) were linked with porosity and lack of fusion.

The VED values were obtained using the following equation [10]:

$VED = \frac{P}{S*HS*LT}$; where P is the laser power, S is the scanning speed, HS is the hatch spacing, and LT is the layer thickness.

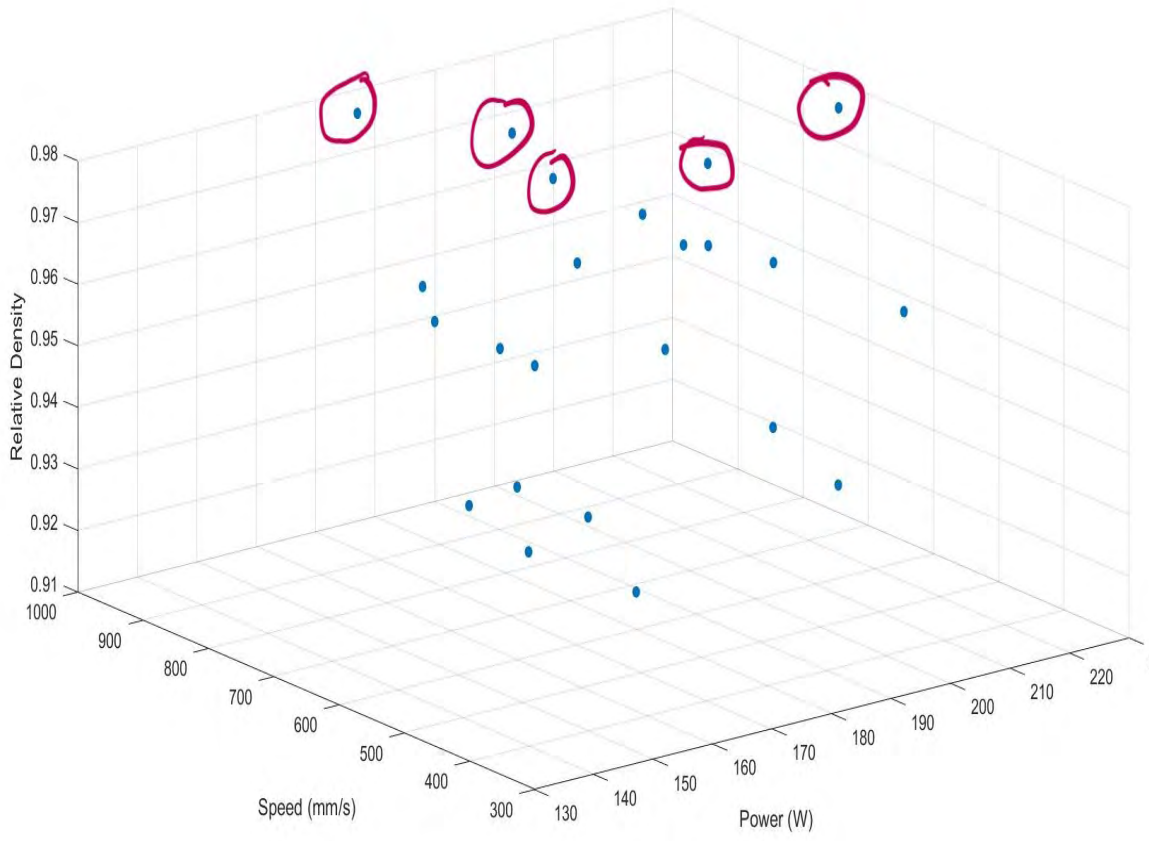

Figure 2.6: Scanning speed, power, and RD plot of all printed samples

The sample parameters and corresponding RD values are summarized in table 2.4 below.

Table 2.4
Summary of the chosen parameter of highest RD.

Parameters	**Numerical Values**
Sample Name	A , F , H, ,J , K
Power (W)	152, 203, 177, 152, 177
Corresponding Scanning Speed(mm/s)	300, 700, 1000, 500, 500

Corresponding RD (%)	97.6, 97.5, 97.6, 96.4, 97.7
Corresponding VED (J/mm^3)	506.67, 290, 177, 304, 354

Relative density of 96% and above was achieved at the printing parameters listed on Table 2.4 above. Yet, RD by itself was an insufficient measure to determine the optimal printing parameters. The following subsection will discuss the microstructural changes observed in as-printed, HIP and HIP + HT samples.

2.3.2 H13 as-printed samples

Figure 2.7 shows images of the microstructures of 11 samples having relative density values of %93 or greater. Even though samples exhibit high RD values, cracks are voids are seen among most samples.

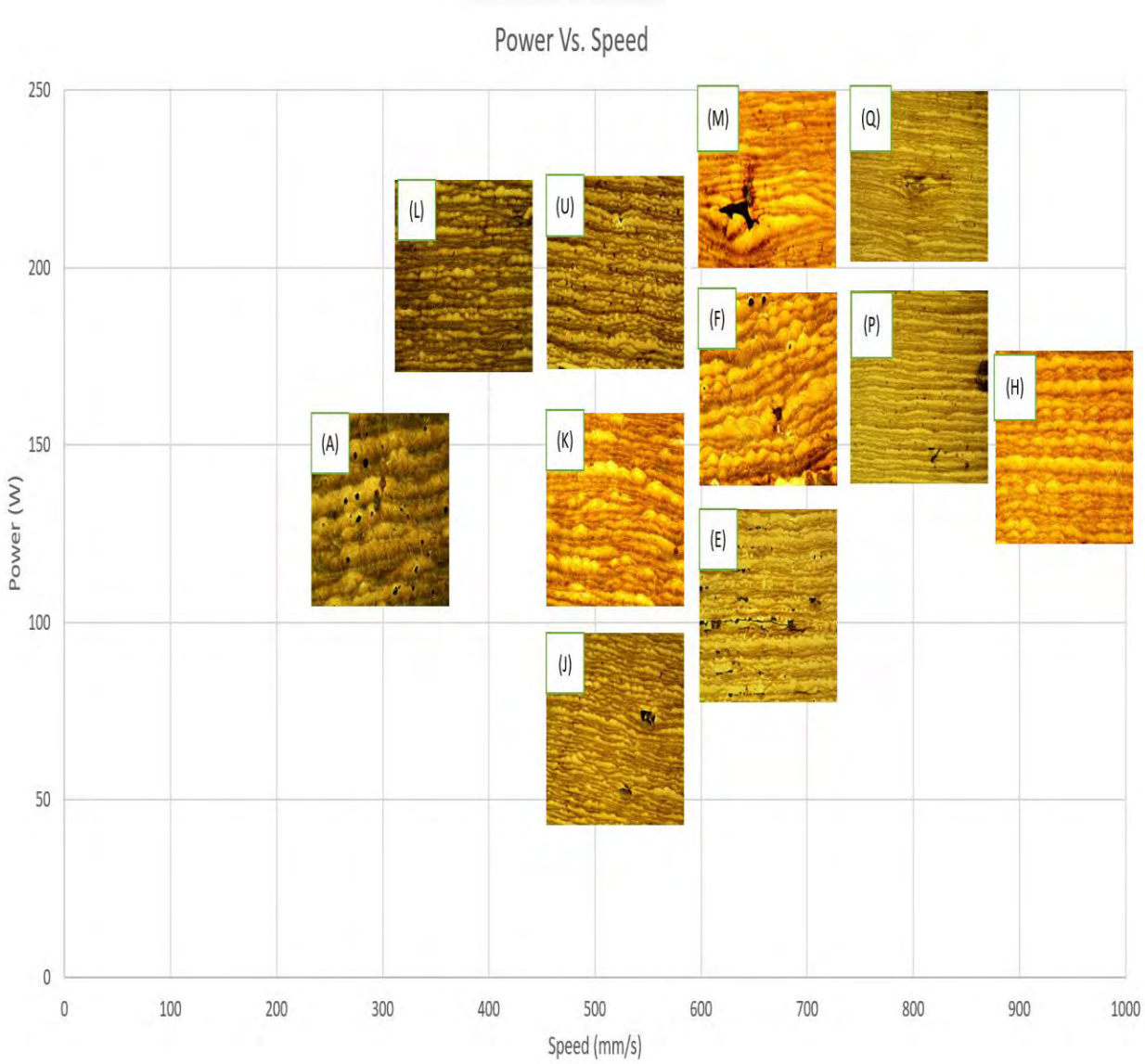

Figure 2.7: microstructures of samples having RD > %93.

As seen in figure 2.7, a laser power value higher than 203W with scanning speed lower than 600 mm/s generates porous samples with cracks and lack of fusion (LOF). Figure 2.8 below shows close-up images of samples A, L, U, and M.

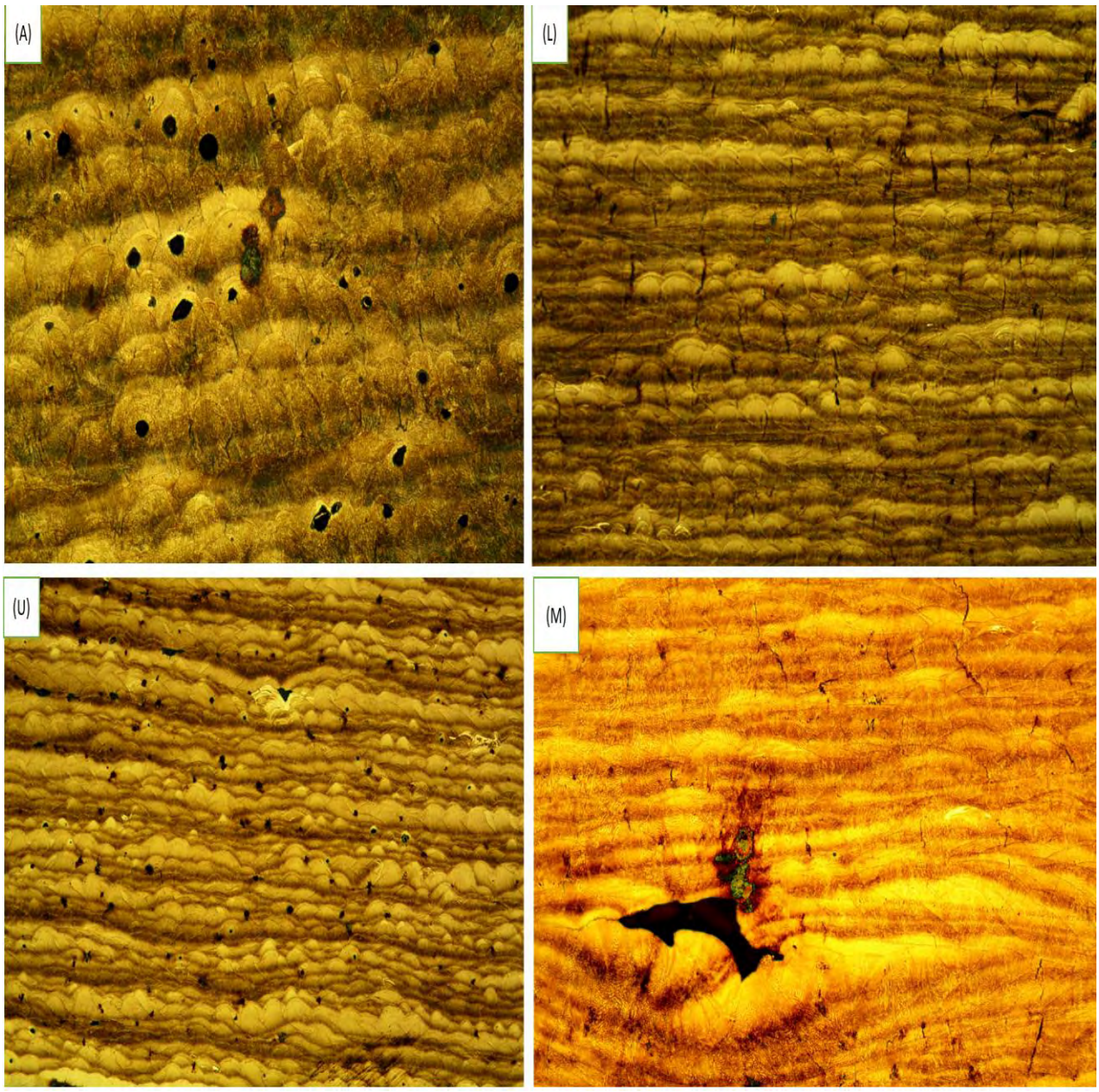

Figure 2.8: high laser power and low speed effects on samples

The cracks and pores observed in the samples shown in figure 2.8 can be attributed to the amount of residual stress where it is found that H13 samples with RD values between 93 to 96% experience a large amount of residual heat [11]. Laser power is the main contributor of energy that goes into fusing the particles. While having too high laser power value can result in a high amount of residual heat, low laser powers can result in lack of fusion [12]. This phenomenon was observed in one of the samples with low laser power and is shown in figure 2.9.

Figure 2.9: sample with low laser power showing LOF.

On the contrary, the following laser power and scanning speed parameter combinations exhibited less cracks and voids: (K)177W with 500mm/s, (F) 203W with 700 mm/s, and (H)177W with 1000 mm/s. Figure 2.10 shows SEM images of the three mentioned samples. While the samples exhibit few cracks and pores, it is important to notice that increasing the scanning speed to 1000 mm/s resulted in powder particles being un-melted as seen in samples H.

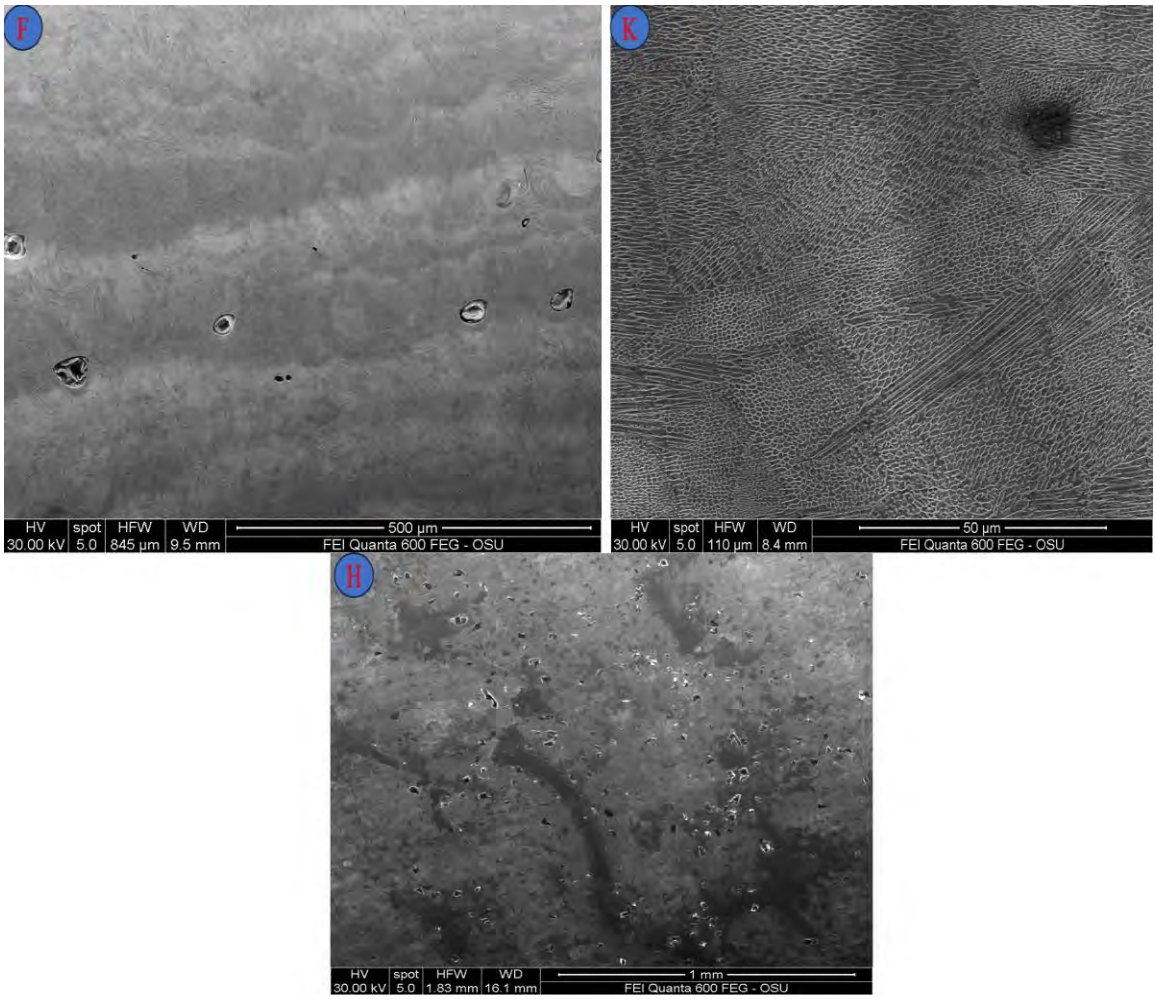

Figure 2.10: samples F, K and H showing few cracks and pores.

An EDS image was taken from sample H to further investigate the nature of the particles shown in figure 2.10. It is concluded that they were chromium (Cr), vanadium (V), molybdenum (Mo) particles that were not fully fused as shown in figure 2.11.

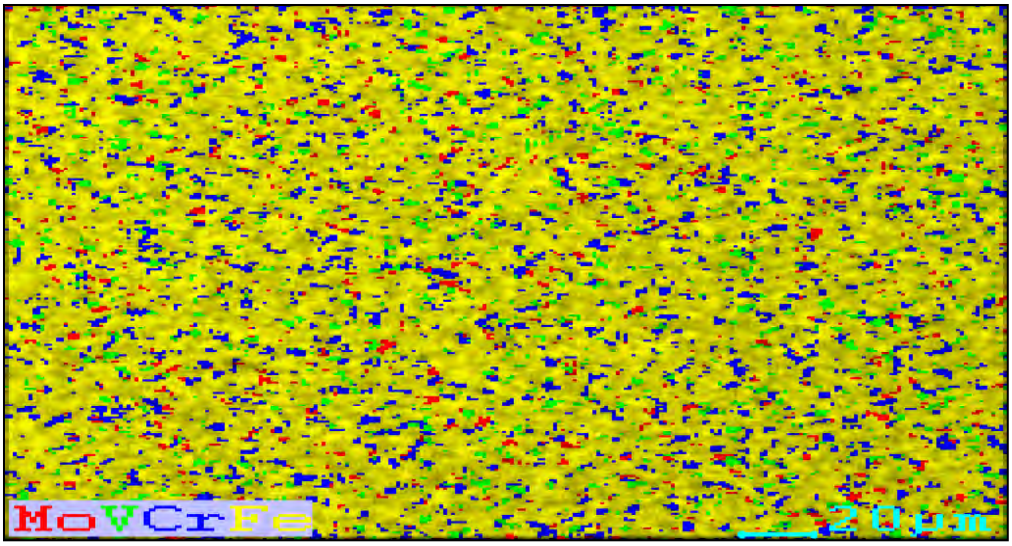

Figure 2.11: EDS image of sample H

Based on the RD values listed on Table 2.4 and SEM of samples with least number of cracks, the following samples are selected to apply HIP and HT on: A, F, J, K, H. The goal of applying HIP and HT is to observe microstructural changes. The results are discussed in the following subsection.

2.3.3 HIP effects

Hot isostatic pressing is a method used to treat cracks by applying heat and pressure to a specimen. Even though HIP is a process that can potentially cure microcracks, it is an ineffective method when it comes to larger cracks, keyholes, and lack-of-fusion [13]. With that idea in mind, sample A, F, J, K and H were selected for the HIP process since they had the least number of cracks visible.

In this experiment, the HIP parameters are: temperature of 1163°C, a pressure of 102 MPa and pressing time of 3 hours. The resulting relative density values of HIP samples and the as-printed samples are listed in table 2.5 below.

Table 2.5: RD values of HIP and as-printed samples

Sample	HIP RD	As Printed RD
A	%93.33	%97.60
F	%98.03	%97.54
H	%90.53	%97.62
J	%93.83	%96.43
K	%92.56	%97.77

It is observed that sample A, H, J and K have seen a reduction in their relative density value, while sample F increased by approximately %0.5. The lowering of RD in sample A, H, J and K was accompanied with noticeable defects on the microstructures that will be discussed in the next paragraph. The negative impacts can be linked to the amount of heat applied in the HIP process.

A HIP temperature of 1163°C was found to be too high. In a previous study, it was concluded that 1020°C and 2 hours of pressing time were ideal in curing cracks [14]. In this experiment, the temperature and pressing time were high in comparison and they led to the worsening of microstructures of 4 out of 5 samples. A comparison of samples showing the defects after HIP is shown below in figure 2.12.

One the left-hand side of figure 2.12, four samples are shown to have some pores with few cracks and keyholes. The goal of HIP was to reduce pores and increase RD, however, opposite results can be seen on the right-hand side of the figure.

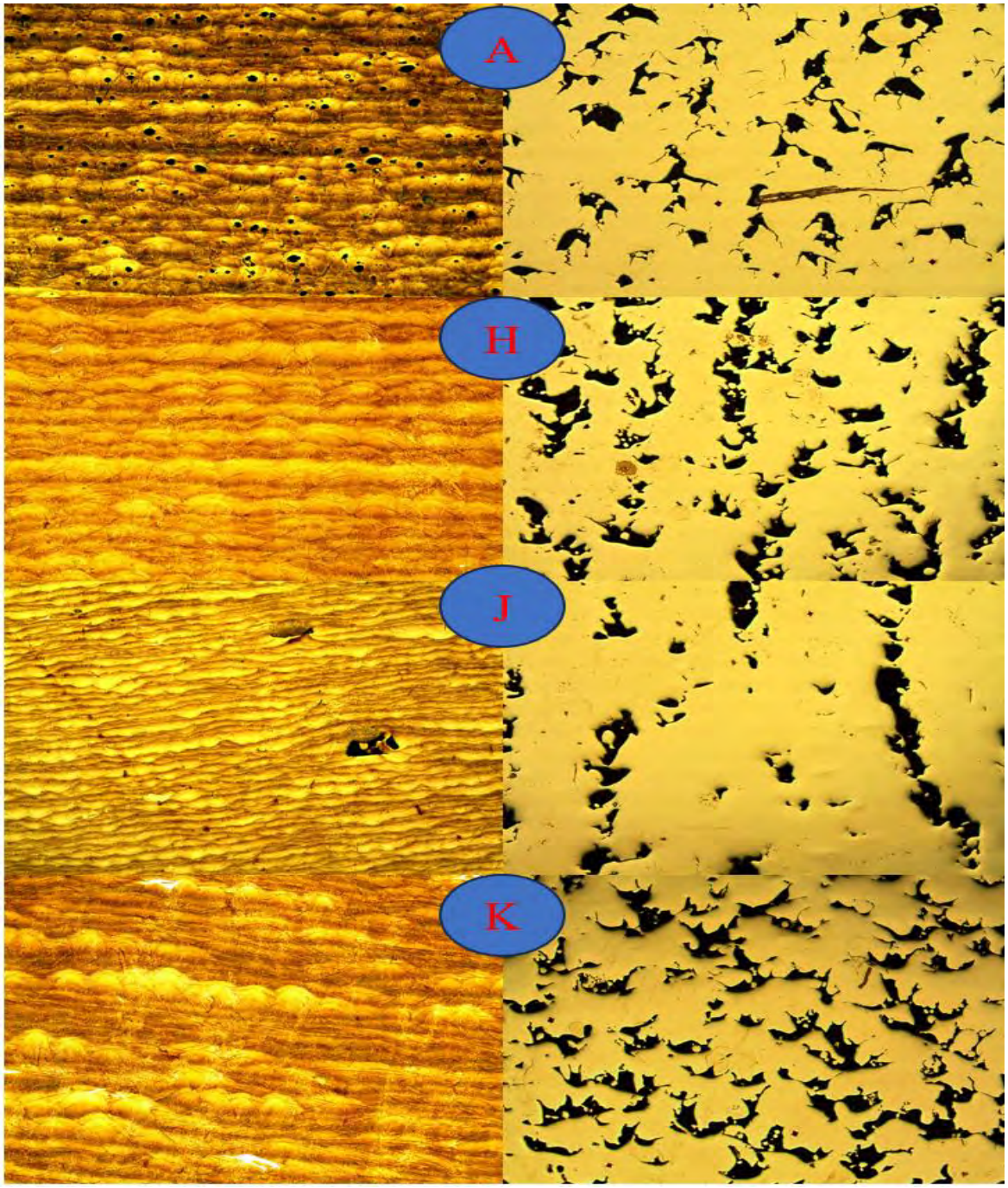

Figure 2.12: microstructure of sample A, H, J and K showing defects on the right-hand side, and images of as printed on the left-hand side.

On the contrary, sample F did indeed have higher RD and less pores after HIP. Figure 2.13 shows the results on sample F, where the microstructures visibly have fewer pores and cracks.

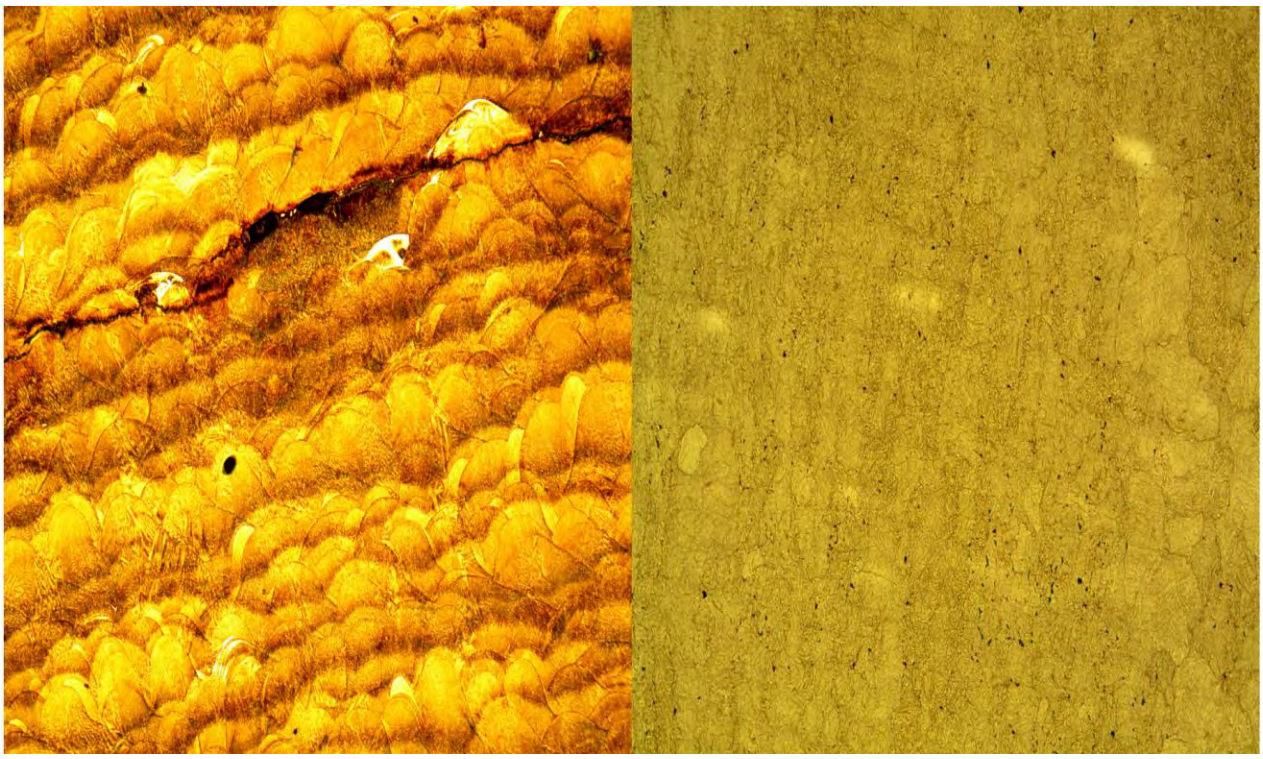

Figure 2.13: sample F's showing as printed microstructure on the left-hand side, and after HIP on the right-hand side.

Based on the results shown on table 2.4 and figure 2.13, the specimen (sample F) had less porosity after the HIP process. A heat treatment was carried out with the goal of altering the metallurgical properties of the H13 sample [15]. The results of the heat treatment will be discussed in the following subsection.

2.3.4 HIP and heat treatment effects

Obtaining a full martensitic microstructure was the goal of heat treatment as it is shown to improve the mechanical properties of H13 for its intended purposes [10]. The specimens were heated to 1160˚C for two hours then were quenched in water, followed by an aging process at 550˚C, 650˚C for an hour at each temperature. The heating process increased the grain size, but the rapid cooling decreased the size and caused recrystallization of grains as shown in figure 2.14 [16].

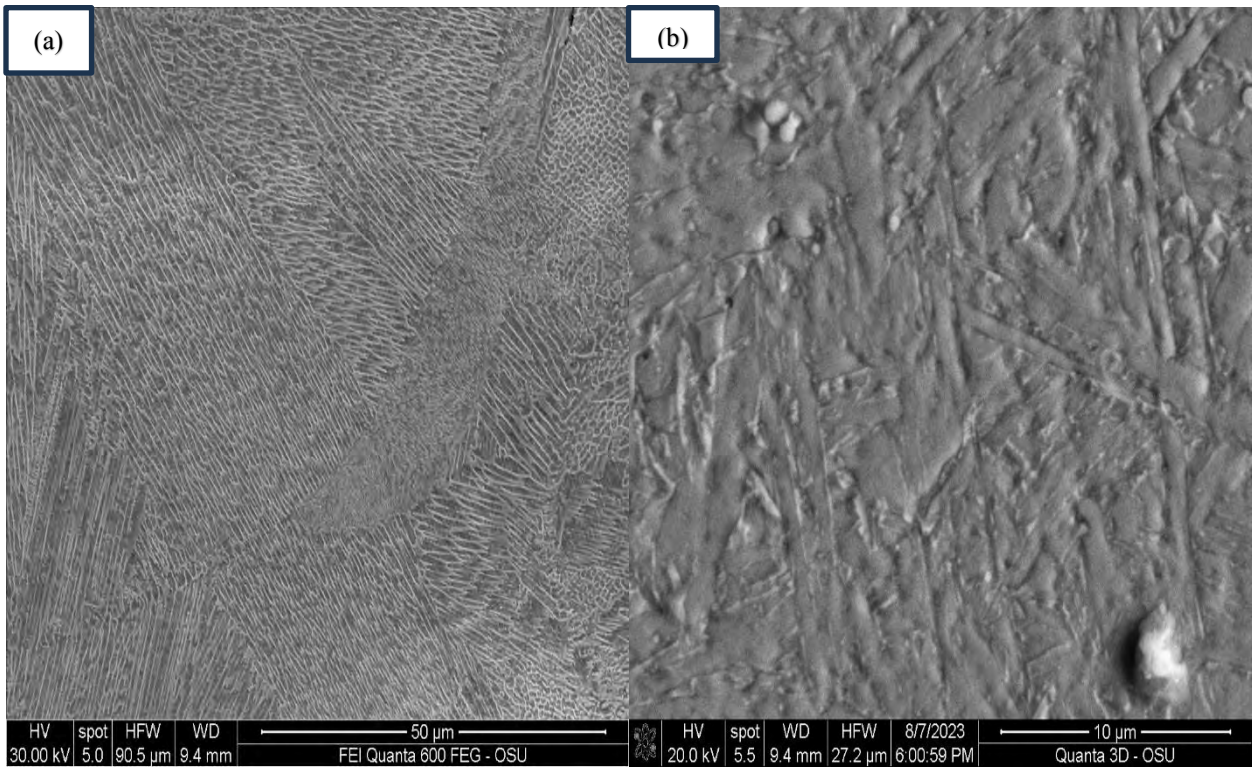

Figure 2.14: SEM images of sample F showing before and after HIP+HT in (a) and (b) respectively.

2.3.5 microhardness hardness measurements

The highest microhardness, 646Hv, in the as-printed set was achieved in sample F, with the corresponding parameters: 203W, 177mm/s, 40µ HS, and 25µ LT. The hardness of sample F was reduced to 566Hv after the HIP process. The %12 reduction in microhardness after HIP can be attributed to the temperature used. 1163℃ is found to be a high temperature that allowed grain growth and recrystallization of crystals [14].

The process of tempering reduced the microhardness of sample F even further. Three different tempering setups showed significant decrease in the microhardness obtained from as-printed sample. Table 2.6 shows the changes of microhardness associated with each tempering setup.

Table 2.6: microhardness values of sample F, with variations of tempering temperatures.

Tempering set-up	as-printed (Hv)	Tempered (Hv)	Reduction %
550°C, for 2 hours	646.4	433.4	32.95%
650°C, for 2 hours	646.4	308.04	52.35%
550°C+650°C, for 1 hours each	646.4	385.34	40.39%

The reduction in microhardness as shown in table 2.6 is proportional to the tempering temperature. This can be linked to the grain growth influenced by the heat applied, as grains get larger with higher temperature. This leads to dislocations traveling longer distances before they are stopped by a grain boundary [14]. This correlation between the tempering temperature and microhardness is proved in table 2.6. The first setup shows the lowest reduction in hardness (%32.95), while the second setup shows the highest reduction (52.35%).

2.4 Conclusion

A list of 27 printing parameters were investigated and a candidate process parameter for LPBF was optimized for powder H13 tool steel. The effects of laser power and scanning speed on the microstructures and mechanical properties of H13 printed samples were also analyzed. The highest microhardness was reached at sample F, where a relative density of 97% was achieved. Hot isostatic processing and heat treatment were applied, and they resulted in a slight increase of RD but at the expense of microhardness. Post Processing cured some of the defects in sample F but generated more defects in other samples. A list of the findings is as follows:

- Several parameters generated relative densities above 97%. The corresponding parameters are A (152W, 300mm/s), E (177W, 700mm/s), F (203W, 700 mm/s), H (177W, 1000mm/s), K (177W, 500mm/s), and M (225W, 700mm/s). The highest hardness was achieved at parameter F, at a value of 646.4 Hv and

a VED value of 290 J/mm$^{3.}$ Keyhole, porosities are cracks were predominantly found in samples of VED above 300 J/mm^3 and below 200 J/mm$^{3.}$

- Hot isostatic pressing was applied to sample F, and it increased the RD by 0.5%. However, the HIP parameters (1163℃ ,102 MPa and 3 hours) resulted in worsening of microstructures of sample A, H, J and K. As found in the literature, a temperature value of 1020℃ was adequate to increase the RD, while increasing the temperature above 1020℃ resulted in more cracks due to the residual heat [14]. Even though the HIP process increased the RD of sample F, it did decrease its microhardness by 12%.
- Water quenching was applied to sample F, followed by 3 heat tempering setups. Recyclization of crystals was observed, and further decrease of microhardness was observed when the tempering temperature was at 650℃. The 550℃ tempering temperatures had less microhardness reduction than the other two setups. The microhardness reduction was resulted by the recrystallization of microstructures and grain growth due to the heat applied.

Chapter 3. Conclusion and Future Work

3.1 Conclusion

H13 tool steel was fabricated via laser powder bed fusion process. Initially, a total of 27 parameter combinations were investigated, but were later narrowed down to five. A summary of the selected five parameter combination is shown below:

Table 3.1: reiteration of results obtained from section 2.3.

Parameters	Numerical Values
Sample Name	A , F , H, ,J , K
Power (W)	152, 203, 177, 152, 177
Corresponding Scanning Speed(mm/s)	300, 700, 1000, 500, 500
Corresponding RD (%)	97.6, 97.5, 97.6, 96.4, 97.7
Corresponding VED (J/mm^3)	506.67, 290, 177, 304, 354

Based on the results shown in table 3.1, samples A, F, H, J and K had relative densities greater than 96% in the as-printed state. However, the results also showed high defects in samples having a VED value greater than 300 J/mm^3, and in samples having VED lower than 200 J/mm^3.

HIP process was applied to cure the microcracks, but an opposite effect was observed. The appearance of large cracks was observed after HIP, and this phenomenon can be linked to the temperature used (1163 ˚C). As previously shown in the literature [14]; while 1020 ˚C is an adequate temperature in healing microcracks, exceeding it can result in worsening effects.

Water quenching and tempering was only carried out for one sample, F. The purpose of selecting sample F was based on its slight increase in the relative density, as opposed to the other four samples. Water quenching and tempering showed recrystallization of grain and grain growth. The effects of grain growth showed a decrease in the microhardness of the sample by up to 52%.

3.2 Future Work

Several printing parameters and post processing methods on H13 tool steel via LPBF were discussed in this study. The study, however, lacks key findings on the effects on other mechanical properties associated with the optimized parameters. Several areas of future work will be addressed.

Dog-bone sample, according to the ASTM D638 standard, is one area that could be investigated. The ASTM D638 standard is a guide that provides key findings on the tensile strength, modulus of elasticity and elongation. Dog-bone samples of different parameter sets, and post processing methods could give numerical comparisons between printed samples.

Finally, the correlation between chamber vacuum and cooling system could be investigated. To elaborate, the OR Laser Creator, which was used to conduct this study, would reach a temperature of 38˚C about half-way through the printing process. To avoid overheating, the OR Creator would be paused to allow the temperature to drop below 38˚C. This repeated pausing-resuming cycle led to a visible distortion on the printed samples. The elimination of residual heat through an improved vacuum and cooling system is one area for future work.

References

[1] Razzaq, Asif, et al. "Investigating the asymmetric linkages between infrastructure development, green innovation, and consumption-based material footprint: Novel empirical estimations from highly resource-consuming economies." *Resources Policy* 74 (2021): 102302.

[2] Namoun, Abdallah, et al. "Solid waste generation and disposal using machine learning approaches: a survey of solutions and challenges." *Sustainability* 14.20 (2022): 13578.

[3] Paris, Henri, et al. "Comparative environmental impacts of additive and subtractive manufacturing technologies." *CIRP Annals* 65.1 (2016): 29-32.

[4] Kruth, J-P., Ming-Chuan Leu, and Terunaga Nakagawa. "Progress in additive manufacturing and rapid prototyping." *Cirp Annals* 47.2 (1998): 525-540.

[5] Sepasgozar, Samad ME, et al. "Additive manufacturing applications for industry 4.0: A systematic critical review." *Buildings* 10.12 (2020): 231.

[6] Baba, Toshiyuki. "Progress of the dies and molds industry and the role of the German immigration network in Brazil: Case studies in ABC districts in Sao Paulo, Resende, and Joinville." (2018).

[7] Yang, Xin, et al. "Microstructure evolution and mechanical properties of H13 steel produced by Selective Electron Beam Melting." *Materials*

[8] Gordon, Jerard V., et al. "Defect structure process maps for laser powder bed fusion additive manufacturing." *Additive Manufacturing* 36 (2020): 101552.

[9] https://www.carpentertechnology.com/alloy-finder/h13 [accessed 2023August]

[10] Katancik, Michael, et al. "Selective laser melting and tempering of H13 tool steel for rapid tooling applications." *Journal of Alloys and Compounds* 849 (2020): 156319.

[11] Narvan, Morteza, et al. "Part deflection and residual stresses in laser powder bed fusion of H13 tool steel." *Materials & Design* 204 (2021): 109659.

[12] Yang, Xuan, Yazhi Li, and Biao Li. "Formation mechanisms of lack of fusion and keyhole-induced pore defects in laser powder bed fusion process: A numerical study." *International Journal of Thermal Sciences* 188 (2023): 108221.

[13] AlMangour, Bandar, Dariusz Grzesiak, and Jenn-Ming Yang. "Selective laser melting of TiB2/H13 steel nanocomposites: Influence of hot isostatic pressing post-treatment." *Journal of Materials Processing Technology* 244 (2017): 344-353.

[14] Maistro, Giulio, et al. "Quenching and hot isostatic pressing of additively manufactured tool steel." *Available at SSRN 3785874* (2021).

[15] Ramezani, Maziar, et al. "Evaluation of carbon diffusion in heat treatment of H13 tool steel under different atmospheric conditions." *Journal of Materials Research and Technology* 4.2 (2015): 114-125.

[16] Al-Qawabeha, Ubeidulla F. "Effect of heat treatment on the mechanical properties, Micro hardness, and impact energy of H13 alloy steel." *International Journal of Scientific & Engineering Research* 8.2 (2017): 100-104.

[17] Narvan, Morteza, Kassim S. Al-Rubaie, and Mohamed Elbestawi. "Process-structure-property relationships of AISI H13 tool steel processed with selective laser melting." *Materials* 12.14 (2019): 2284.